Processing and Classification of Biological Images: Application to Histology

Bruno Nunes & Luís Miguel Rato
Departamento de Informática
CITI - Centro de Investigação em Tecnologias de Informação da Universidade de Évora
Universidade de Évora, Évora, Portugal

Fernando Capela e Silva
Departamento de Biologia
Instituto de Ciências Agrárias e Ambientais Mediterrânicas (ICAAM)
Universidade de Évora, Évora, Portugal

Ana Rafael & António Silvério Cabrita
Instituto de Patologia Experimental, Faculdade de Medicina da Universidade de Coimbra
Universidade de Coimbra, Coimbra Portugal

ABSTRACT: *This article deals with a histological problem by using image processing and feature extraction in images of renal tissues of rats and their classification through various methods such as: Bayesian inference, decision trees and support vector machines.*

Keywords: *Image Processing, Segmentation, Classification, Kidney, Renal Glomeruli, Histology, Feature Extraction, Xenobiotics*

1 INTRODUCTION

The observation in photonic microscopy of histological sections allows us to evaluate the structural changes of an individual's exposure to xenobiotics.

This evaluation can be made through quantitative criteria by using computational tools and algorithms to make the process faster and more accurate.

2 OBJECTIVES

This work intends to evaluate the morphological changes in the kidney of rats, caused by exposure to xenobiotics, through computer-assisted histomorphometric analysis.

3 IMAGE PROCESSING

In this work, we used 210 kidney photomicrographs of 21 Wistar rats belonging to three groups: Group I [Control, n=7], Group II [Pesticide Thiram, n=6) and Group III [Corn Oil, n=8] (Fialho et al. 2001).

Samples were collected after 35 days of testing and processed by histological routine techniques, in Instituto de Patologia Experimental, Faculdade de Medicina da Universidade de Coimbra.

The final preparations were observed with a Nikon Eclipse 600 microscope, using a magnification of 200X, and the images were acquired using a Nikon DN100 digital camera.

For each animal of each group was selected a section and, for each of them, there were randomly observed 10 renal corpuscles (Figure 1).

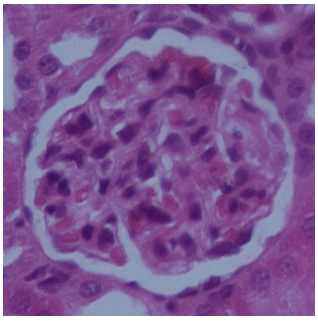

Figure 1: Example of a renal corpuscle

The images were then processed using several tools from the program *ImageJ* (Rasband 2009) together with an existing plugin called *MultiCell Outliner* (MCO) (Latxiondo 2006), in order to highlight the renal corpuscles.

3.1 *METHODOLOGY*

The methodology we used was divided in two different steps: the delimitation and the extraction of the renal corpuscle.

3.1.1 *DELIMITATION*

In this first step, the objective was to define the contour of the renal corpuscle and fill it's interior.

Depending on the three complexity degrees of the images: low, medium and high, there were different types of approach.

Low Complexity Images

We say that an image has a low complexity degree when the Bowman's capsule is clearly visible and without any breaks, as we can see in Figure 2.

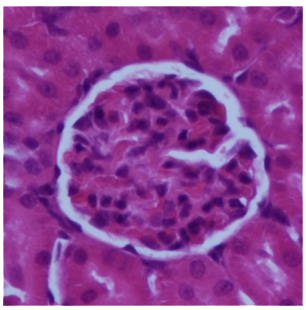

Figure 2: Low complexity renal corpuscle

In these cases, we were able to fully trace the outline of the renal structure using only the MCO plugin, as left image from Figure 3 shows.

Once the outline is highlighted, we've painted it's interior with the black color, using the *Fill* tool, as shown in the right image from Figure 3.

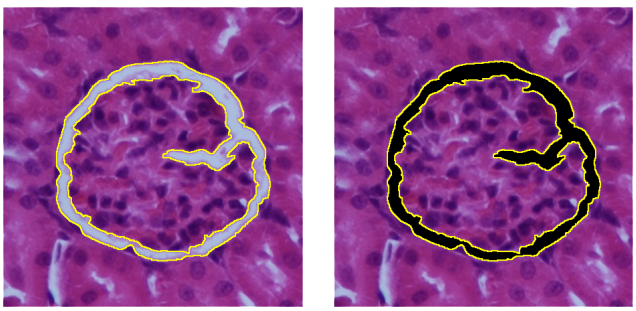

Figure 3: Delimitation and filling of a low complexity renal corpuscle

The result from a low complexity image delimitation is shown in Figure 4.

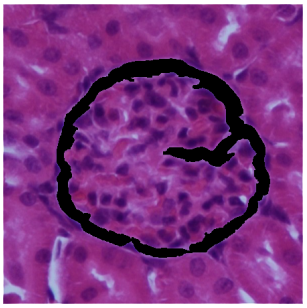

Figure 4: Final result from a delimitation in a low complexity image

Medium Complexity Images

In images with a medium complexity degree, despite it contains some breaks, the Bowman's capsule shape is perfectly recognizable.

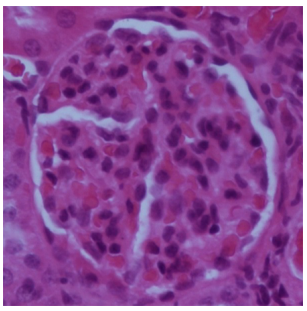

Figure 5: Medium complexity renal corpuscle

In these cases, we only managed to outline the renal corpuscle partially using MCO plugin. The following figure shows the partial delimitation step by step.

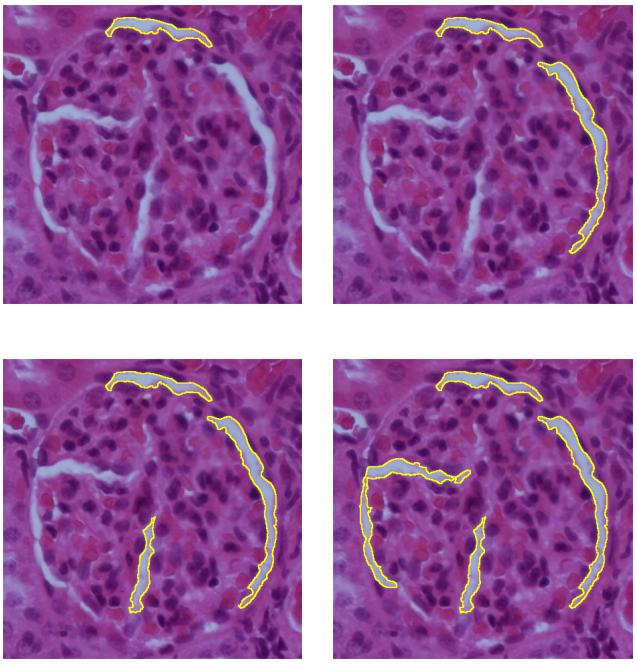

Figure 6: Partial delimitation of a medium complexity renal corpuscle

After the partial delimitation was completed, the inside of each highlighted part was painted with the black color using the *Fill* tool.

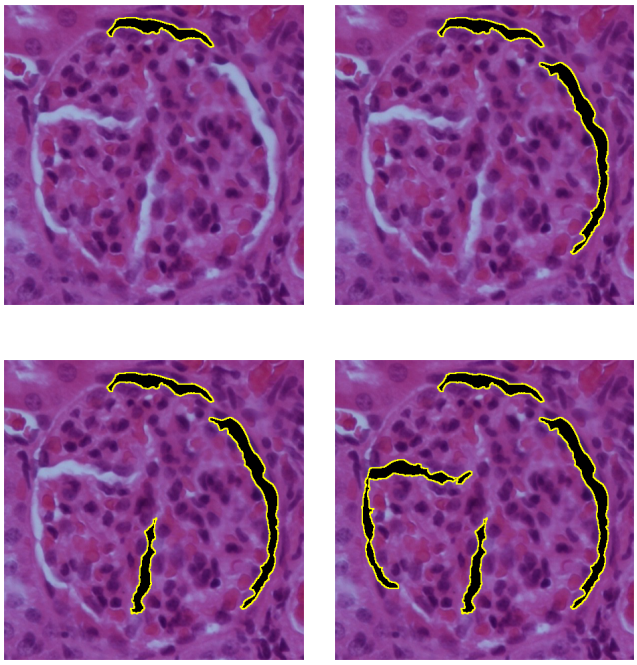

Figure 7: Filling the partial delimitation of a medium complexity renal corpuscle

The following figure shows the result after the partial delimitation of the renal corpuscle.

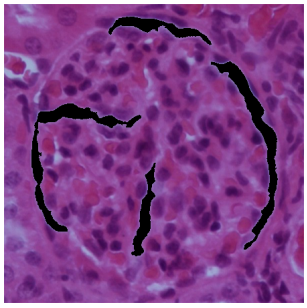

Figure 8: Partial delimitation in a medium complexity case

To complete the process, it was necessary to manually finish the Bowman's capsule's contour, using the brush tool with 3 pixels size.

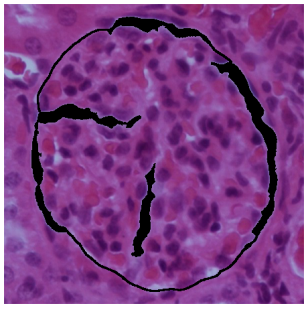

Figure 9: Final result from the complete delimitation of a medium complexity renal corpuscle

High Complexity Images

Images with high complexity degree are the worst case scenario. In these images, the Bowman's capsule's shape is difficult to identify or barely can be seen.

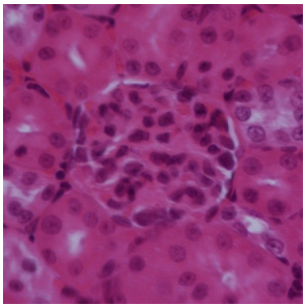

Figure 10: High complexity renal corpuscle

We didn't obtained satisfactory results using the MCO plugin in these cases, so the renal corpuscle had to be entirely delimited by hand, using the brush tool with 3 pixels size. The delimitation steps and the final result can be seen in figure below.

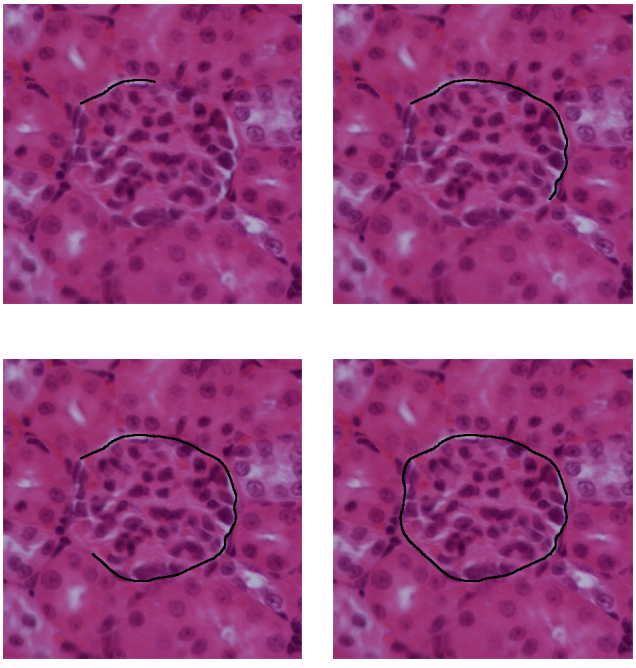

Figure 11: Delimitation of a high complexity renal corpuscle

3.1.2 *EXTRACTION*

In the second step, the objective was to isolate the regions painted in black previously, under the form of binary images.

To do this, we've made a RGB to Grayscale conversion, as can be seen in Figure 12.

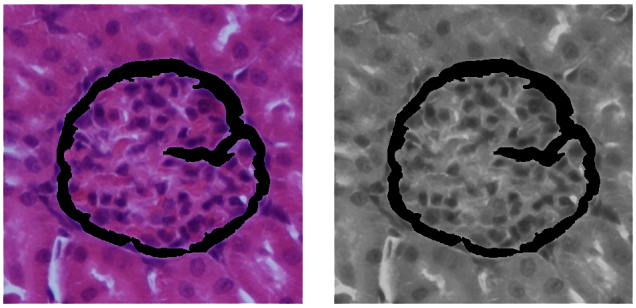

Figure 12: RGB to Grayscale conversion

After this conversion, each of the image's pixels stops storing an RGB color value and starts to store a gray intensity, being the strongest intensity the black color and the weakest intensity the white color.

Then we've applied the threshold technique on top of the grayscale image, in order to highlight the renal corpuscle silhouette, as shown in Figure 13.

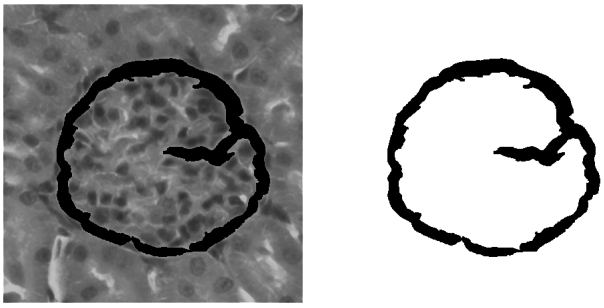

Figure 13: Highlight of renal structure through threshold technique

4 FEATURE EXTRACTION

After isolating the renal corpuscles, and based on the resulting images from processing and segmentation, we used *ImageJ* again to measure several morphological features that served to identify and distinguish the renal corpuscles.

The following features were considered:

Figure 14: Diameter and Perimeter of Bowman's capsule

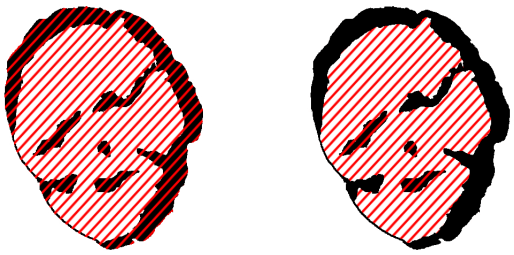

Figure 15: Bowman's capsule's and glomeruli's total area

Figure 16: Exterior and interior Bowman's space

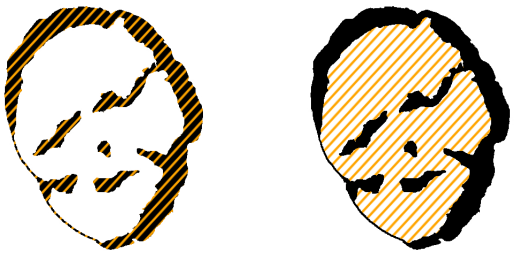

Figure 17: Total Bowman's space and glomerular capillaries area

In addition to these features, we've also considered the fractal dimensions of the renal corpuscle.

Finally, after measuring all these features for the complete set of images, the resulting data was stored in the form of a vector of features for each image.

5 CLASSIFICATION

Once the entire data set was obtained, we applied several algorithms for classifying data using *WEKA* (Witten and Frank 2005). The used classifiers were:

- Zero Rule
- One Rule
- Naive Bayes
- J48 Tree
- Support Vector Machines

The classification results, with and without feature selection, may be seen in Table 1.

Table 1: Percentage of accuracy rate of the different classifiers

Classifier	No Selection	Selection
Zero Rule	71,3636	71,3636
One Rule	70,4545	72,7273
NaiveBayes	64,5455	73,6364
J48 Tree	70,4545	73,1818
SVM	69,0909	78,1818

In order to reduce uncertainty in the final results we made some transformations on the data, namely the aggregation of image data concerning to the same animal.

The classification results after aggregation of instances, with and without feature selection, may be seen in Table 2.

Table 2: Percentage of accuracy rate of the different classifiers with instance aggregation

Classifier	No Selection	Selection
Zero Rule	71,4286	71,4286
One Rule	66,6667	66,6667
NaiveBayes	85,7143	85,7143
J48 Tree	71,4286	66,6667
SVM	76,1905	80,9524

Comparing the results there have been some improvements on some classifiers, however, a high accuracy rate not always means a good classification. This can be observed through the example of Tables 3 and 4, corresponding to Naive Bayes and Zero Rule confusion matrices, both with feature selection and instance aggregation.

Table 3: NaiveBayes confusion matrix

Classified as →	Healthy	Pesticide
Healthy	12	3
Pesticide	0	6

Naive Bayes has 85,7143% of accuracy rate and correctly classifies all the pesticide instances and the most of the healthy instances.

Table 4: Zero Rule confusion matrix

Classified as →	Healthy	Pesticide
Healthy	15	0
Pesticide	6	0

On the other hand, Zero Rule classifies well all the healthy instances but fails completely when classifying the pesticide instances. On this case, the high accuracy rate (71,4286%) is purely justified with the existence of more healthy instances then pesticide instances.

One way to avoid these type of misunderstandings, it's to consider other variables such as false positive rate and precision of the class of interest. The table below shows values from both variables for each classifier.

Table 5: FP Rate and Precisison of the different classifiers with instance aggregation for pesticide class

Classifier	FP Rate	Precision
Zero Rule	0	0
One Rule	0,267	0,429
NaiveBayes	0,200	0,667
J48 Tree	0,333	0,500
SVM	0,200	0,571

Given these facts, when choosing one of the classifiers we should always consider not only it's accuracy rate but also the the lowest false positive rate an the highest precision on the class of interest. Therefore, based on the previous tables, we can conclude that the best classifier options would be NaiveBayes followed by SVM.

6 CONCLUSION

The results of this work may be considered positive since, by analyzing the information obtained through all the process, it was possible to say with an acceptable degree of certainty, whether or not histological changes occured at the level of renal corpuscles. However, given that there remains an uncertainty in the results of some classifiers, improvements can be made by including other image features.

REFERENCES

Fialho, I., F. Capela e Silva, A. Rafael, & A. Cabrita (2001). Effects of tetramethylthiuram disulfide (thiram) on kidney metallothionein expression in rats. In *Biomarkers of Environmental Contamination*, 24-26 September 2001, Póvoa de Varzim, Portugal, pp. 191.

Latxiondo, K. (2006). Multicell outliner. http://rsbweb.nih.gov/ij/plugins/multi-cell-outliner.html. [accessed July-2010].

Rasband, W. S. (1997-2009). *ImageJ*. Bethesda, Maryland, USA: U. S. National Institutes of Health. http://rsb.info.nih.gov/ij/ [accessed July-2010].

Witten, I. H. & E. Frank (2005). *Data Mining: Practical Machine Learning Tools and Techniques* (2nd ed.). Morgan Kaufmann.